Received: 9 February 2021 | Accepted: 26 March 2021

DOI: 10.1002/mmce.22686

RESEARCH ARTICLE

INTERNATIONAL JOURNAL OF RF AND MICROWAVE COMPUTER-AIDED ENGINEERING WILEY

On further enhancing the bandwidth of wideband RCS reduction checkerboard metasurfaces using an optimization algorithm

Akila Murugesan | **Krishnasamy T. Selvan**

Department of Electronics and Communication Engineering, Sri Sivasubramaniya Nadar (SSN) College of Engineering, Kalavakkam, Tamil Nadu, India

Correspondence
Krishnasamy T. Selvan, Department of Electronics and Communication Engineering, Sri Sivasubramaniya Nadar (SSN) College of Engineering, Kalavakkam, Tamil Nadu, India.
Email: selvankt@ssn.edu.in

Abstract

This article reports an optimization procedure for further enhancing the wideband radar cross section (RCS) reduction bandwidth using a checkerboard metasurface (CMS). The improved fruitfly optimization algorithm is used to determine the unit cells dimensions that offer a further enhanced bandwidth. Two previously reported CMSs are chosen: (a) A square-circle pair designed on Rogers 5880 with a thickness of 6.35 mm and (b) a Jerusalem cross pair designed on Rogers 3010 with a thickness of 1.27 mm. First, unit cell (a) is optimized, resulting in an improvement of 7% from the originally reported bandwidth. Similarly, unit cell (b) shows an enhancement of 5%. Because of cost considerations and in the interest of exploring alternative methods, the substrates in both cases are replaced by Taconic TLY-3 with a thickness of 1.57 mm over an air gap of 5 mm. After optimization, this configuration enhances the 10 dB RCS reduction bandwidth substantially to 81% for (a) and 102% for (b). It is also observed that the − 15 dB bandwidth of the Jerusalem cross-based CMS is 48%, which is the widest reported so far. The alternative configurations of (a) and (b) are fabricated and measured. The measurements are in good agreement with the simulation results.

KEYWORDS

bandwidth, checkerboard metasurface, optimization algorithm, wideband RCS reduction

1 | INTRODUCTION

Radar cross section (RCS) reduction of a metallic target is of use in civil and military stealth applications.[1] Ideally, RCS reduction should enable zero detectability of the target cregardless of the incident wave frequency, angles of incidence, and polarization. Given the difficulty of designing an ideal RCS reducer, further bandwidth enhancement of a wideband checkerboard metasurface (CMS) and minimal scattering in the specular direction are addressed in this work. RCS reduction is generally accomplished in two ways: (a) With absorbers[2] and (b) with scatterers.[3] The first way of reducing the RCS is by enclosing the target with radar absorbing materials commonly realized using a Salisbury screen.[4] Although it provides flexibility in the design, the bandwidth offered is very narrow, and the size is relatively large. The other way of reducing the RCS is by scattering the signal away from the specular direction, which can be achieved either by shaping the target or by using metasurfaces. Shaping[5] the target minimizes the RCS but offers a narrow bandwidth. The other way to redirect the incident signal is by metasurface, which is being widely researched in recent times and has shown wideband characteristics. Three types of metasurfaces reported in the literature are (a) phase gradient metasurfaces (PGMSs),[6-8] (b) polarization conversion metasurfaces (PCMS),[9,10] and (c) CMSs.[11-20]

The concept of a phase discontinuity, proposed in Reference 6, explains how the incident energy is diverted to an arbitrary direction through anomalous reflection and refraction. This principle is used in the construction of PGMS. In Reference 7, the PGMS designed using split-ring unit cells attributes the RCS reduction as a result of surface wave conversion and anomalous reflection. An RCS reduction of 6 dB is reported in Reference 8 by using phase gradient arrays oriented in different directions.

The next type of metasurface is PCMS, which converts the polarization of the incident wave into its orthogonal polarization on reflection, resulting in RCS reduction. In Reference 9, a multi 'v' shaped PCM with an extremely wideband RCS reduction is reported.[10] reports a super broadband coded PCMS, which is optimized based on group search optimization algorithm.

The other type of metasurface is the CMS, which reduces the RCS by the principle of destructive interference. Thin AMC-based CMSs for RCS reduction were introduced in Reference 11, where a combination of an AMC and perfect electric conductor (PEC) arranged in a checkerboard pattern reduces reflection in the boresight. However, the bandwidth offered remained narrow. In Reference 12, the authors examined an AMC-PEC pair with an AMC-AMC pair and inferred that the AMC-AMC-based CMS provides a wider bandwidth than the AMC-PEC pair does. Researchers have contributed to enhancing the RCS reduction bandwidth by suitable choice of element combination. Reference 13 reported a 30% bandwidth by maintaining a $180 \pm 30^{\circ}$ phase difference between two AMCs. Theoretical prediction of the grating lobe direction is explained in Reference 14 using a Jerusalem cross-based CMS, which offers a fractional bandwidth of 40%. In Reference 15, an empirical expression for RCS reduction in terms of the unit cell's reflection coefficient and phase is reported. Additionally, it was stated that a $180 \pm 37^{\circ}$ phase deviation is required between unit cells for an RCS reduction of 10 dB. Dual-band RCS reduction using two dual-resonance AMCs was reported in Reference 16 blended CMSs were reported in Reference 17; single- and dual-band AMCs provided a bandwidth of 83%. The bandwidth is further enhanced to 91% by using four AMCs. A bandwidth of 91.5% was reported in Reference 18, where dual- and triple-resonance AMCs are used. Additionally, the cancelation condition of the checkerboard structure was analytically derived using the equivalent transmission line model. The bandwidth of RCS reduction CMSs is enhanced by suppressing the surface wave in Reference 19. A triple-layered RCS reduction CMS is reported in Reference 20, offering a bandwidth of 96%. The authors have reported in Reference 21, a modification to the design criteria while designing CMS on high-loss, low-cost substrate FR4.

From the above literature, the design of CMSs requires two unit cells whose reflection magnitudes are unity and a phase difference of $180 \pm 37^{\circ}$ for a 10 dB RCS reduction. However, designing two unit cells with this phase deviation over a wide bandwidth is difficult because of the phase comparison between the unit cells. As this comparison is time-consuming, the introduction of an optimization algorithm would ease the design procedure. In Reference 22, the optimization-based PCMS design is discussed. It is well known that optimization speeds up the design process.

Various optimization algorithms, such as the genetic algorithm (GA), particle swarm optimization (PSO) algorithm, and ant colony optimization (ACO), have been widely used for solving electromagnetic problems. In Reference 23, GA, PSO, and ACO were applied for element spacing optimization in a linear array, and it was reported that ACO is computationally efficient. In Reference 24, the improved fruitfly optimization algorithm (IFOA) provided faster convergence than that of PSO for an array synthesis problem. Considering the similarity of a metasurface to an array, the authors have chosen the IFOA to be used in the design of unit cells in the view of further enhancing the bandwidth. However, PSO is as efficient as the IFOA for this problem. This work focuses on an IFOA based optimization approach interfacing MATLAB and CST to further enhance the bandwidth of already reported structures.

The major contributions of this work include further enhancement in the RCS reduction bandwidth of already reported broadband structures, the widest 15 dB RCS reduction bandwidth, demonstration of the operational principle of CMS using sinusoidal signals and estimation of the phase deviation condition for 15 dB RCS reduction.

The phase deviation between unit cells is the critical parameter to design CMS, which is derived in Section 2 using the semiempirical relationship reported in Reference 15. A simple demonstration of how this phase shift aids in destructive interference is explained. Section 3 elaborates the optimization procedure to maximize bandwidth, considering the unit cell's phase difference bandwidth. Section 4 describes the elements chosen and its optimized dimensions. The results and discussion are discussed in Section 5.

2 | RELATIONSHIP BETWEEN PHASE DEVIATION AND RCS REDUCTION

In Reference 25, a semiempirical expression is reported for RCS reduction in terms of the reflection amplitude

and phase of two-unit cells with equal and unequal echo areas. Since this work considers similar echo areas and equal amplitudes, Expression (1) is considered here. In the design of any CMS, the phase deviation between the unit cells over the frequency range is an essential parameter. Hence, Expression (1) is rearranged to determine the phase deviation in terms of RCS reduction, for convenience.

$$\text{RCS reduction}, \sigma_R = 10 \log \left[\frac{A_1 e^{jP1} + A_2 e^{jP2}}{2} \right], \quad (1)$$

where A_1 and A_2 are the reflection coefficient amplitudes of the two unit cells and P_1 and P_2 are their corresponding reflection phases.

Without loss of generality, the following assumptions are made: (a) $A_1 = A_2 = 1$, and (b) $P_1 = 0$, where P_2 is obtained from Expression (2):

$$P_2 = \cos^{-1}\left(2*10^{\frac{\sigma_R}{10}}\right) - 1, \quad (2)$$

for example, if the RCS reduction must be 10 dB, then substituting $\sigma_R = -10$ dB into Equation (2) results in a P_2 of 143, which means that a deviation of 37° from 180° is acceptable to maintain a 10 dB RCS reduction. This could be generalized, as in Expression (3), to indicate what the phase deviation, φ, is acceptable from 180° to maintain a specific RCS value.

$$\text{Phase deviation}, \varphi = 180 - \left[cos^{-1}\left(2*10^{\frac{\sigma_R}{10}}\right) - 1 \right], \quad (3)$$

where σ_R has units of dB. $(180 \pm \varphi)°$ is the phase deviation that has to be maintained between the unit cells for a specific level of RCS reduction. Table 1 presents the phase deviation to be maintained for some specific values of RCS reduction.

When the corresponding phase deviation is maintained, the reflection from the alternate AMCs destructively interferes, leading to a minimum signal in the specular direction. A simple demonstration of how

TABLE 1 Phase deviations for the corresponding RCS reductions

RCS reduction	Phase deviation
10 dB	(180 ± 37)°
15 dB	(180 ± 27)°
20 dB	(180 ± 22)°
30 dB	(180 ± 14)°

Abbreviation: RCS, radar cross section.

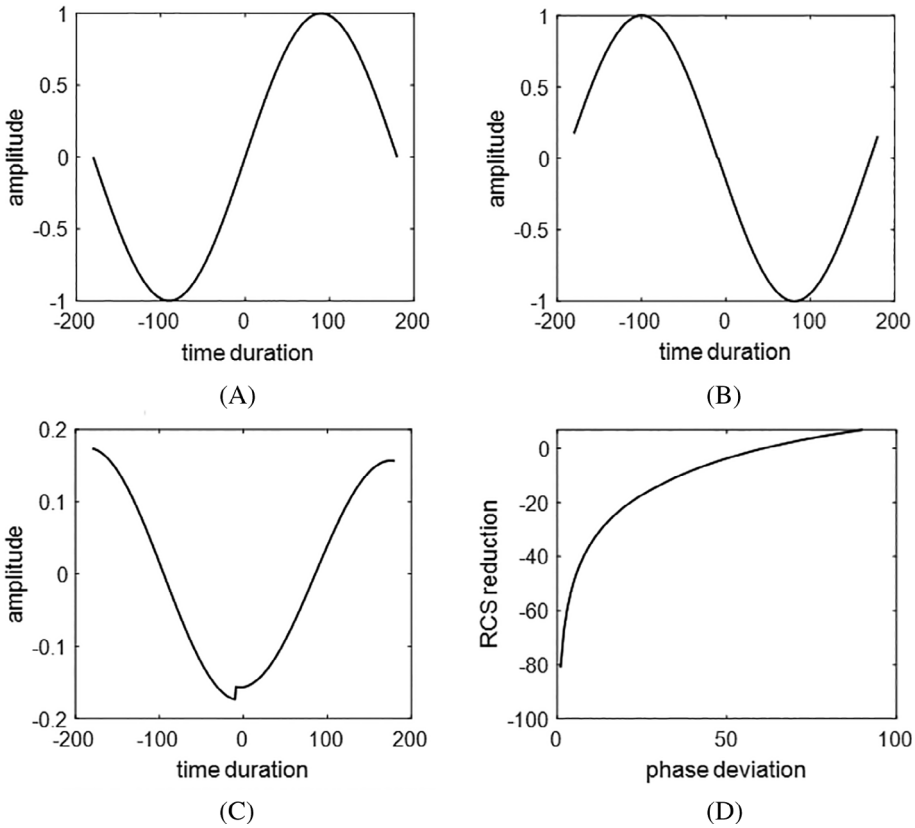

FIGURE 1 Demonstration of destructive interference A, Sinusoidal signal; $s(t)$; B, signal phase shifted, $s(t + 180 + 10)$; C, $s(t) + s(t + 180 + 10)$; D, phase deviation vs radar cross section (RCS) reduction

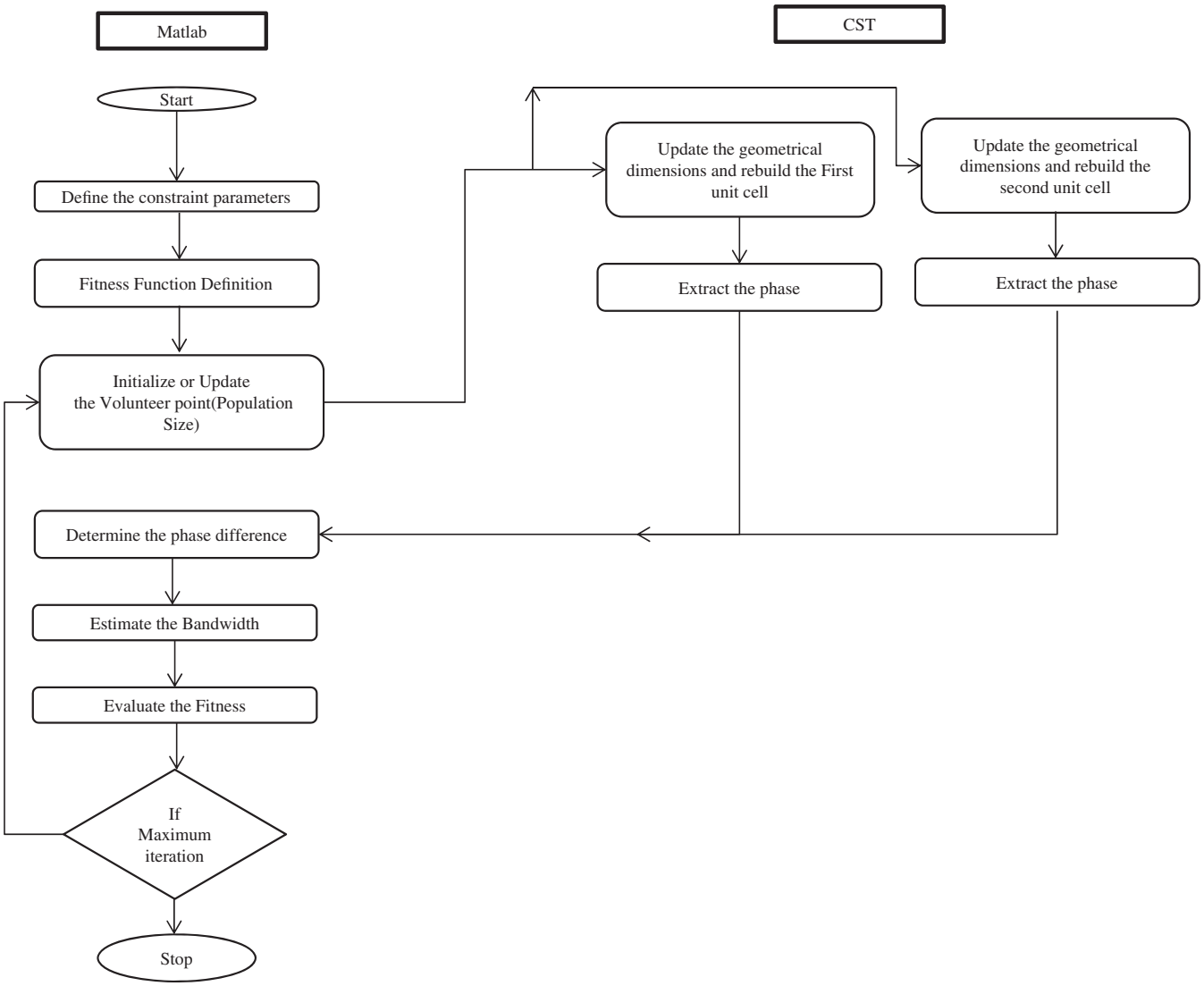

FIGURE 2 Flowchart of the optimization procedure for the unit cell design of checkerboard metasurfaces (CMSs)

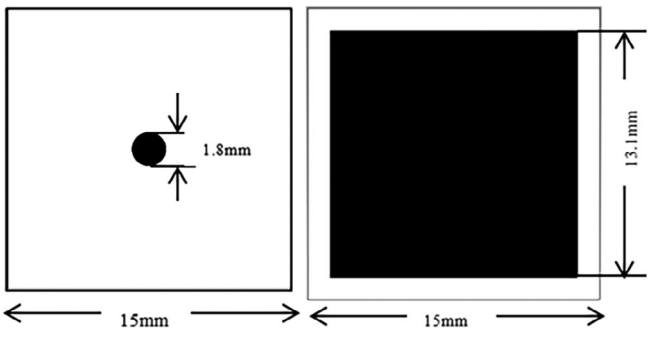

FIGURE 3 Square and circle pair unit cells

destructive interference occurs is illustrated using sinusoidal signals in Figure 1.

Consider a sinusoidal signal, $s(t)$, of frequency f_r, as shown in Figure 1A. The signal is shifted by $180 \pm 10°$, represented as $s(t + 180 + 10)$ in Figure 1B. Figure 1C shows the addition of $s(t)$ and $s(t + 180 + 10)$. The ratio of the peak of the resultant to the peak of the actual sinusoidal signal gives the RCS reduction. Figure 1D shows the RCS reduction vs phase deviation (φ). Notably, when the phase deviation between the unit cells is $(180 \pm 10)°$, the RCS reduction attained is 37 dB.

Manually optimizing the unit cells for the specific phase deviation criteria over a broad frequency range is very difficult and time-consuming; hence, an optimization methodology is proposed in the following section.

3 | OPTIMIZATION METHODOLOGY

The design of a CMS involves the choice of two unit cells whose phase response deviation has to be within

$180 \pm \varphi^{\circ}$ over the entire frequency range. The process of comparing the phase deviation manually to obtain wideband is tedious; hence, an optimization-based approach utilizing both CST and MATLAB is used to further enhance the bandwidth of wideband CMS.

CST and MATLAB are interfaced to design unit cells, and the corresponding codes refer to Reference 26. The IFOA is chosen for design optimization and is coded in MATLAB.

The function of any optimization algorithm is to determine the constrained parameter that satisfies the fitness function. A summary of the IFOA algorithm is as follows

Step 1: *Defining the parameters*: Number of volunteer points, that is, the population size (N), the search coefficient (p), the weight coefficient (α), the initial weight (ω_0), the maximum number of iterations, and the fitness criterion

Step 2: *Initializing the first residential point*:

$X_{\text{Best}} = p$, the search coefficient

Step 3: *Updating the volunteer points*:

$X_i = X_{\text{Best}} + \omega \times \text{random value } (-1, 1)$

$$\omega = \omega_0 \left[\frac{\text{iteration}_{\max}\text{-iteration}}{\text{iteration}_{\max}}\right]^n,$$

n is the weighing order $0 \le n \le 10$,

$$X_{\text{av}} = \frac{\sum_{i=1}^{N} X_i}{N}.$$

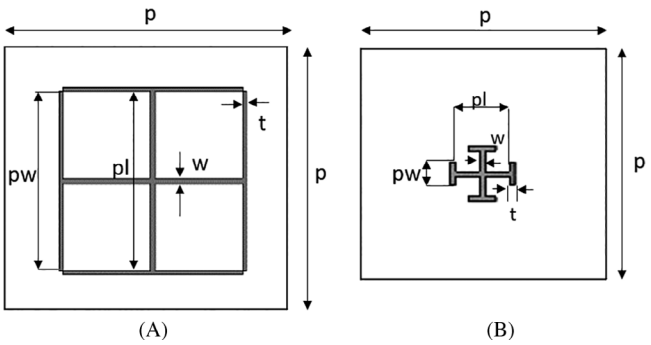

FIGURE 4 Jerusalem cross based unit cells A, small B, large

Step 4: *Calculating the Smell concentration value* (S_i): For each of the volunteer points, the smell concentration value is estimated using the objective function or the fitness function.

S_i = objective function (X_i)

Step 5: *Finding* X_{Best}: The value of X_i which has obtained the maximum S_i is chosen as X_{Best}

Step 6: *Iterative procedure*: Repeat step (3) to (5) over the entire search space until the maximum number of iterations is reached or the fitness criterion is met.

The volunteer points are the constrained parameter, which is the dimension of the unit cell, and the fitness function is the phase difference bandwidth between the unit cells. The optimization procedure starts by

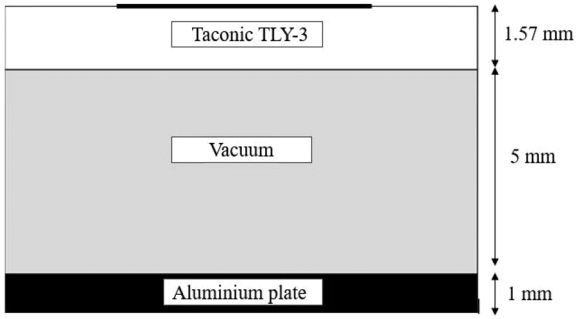

FIGURE 5 Side view of the altered structure

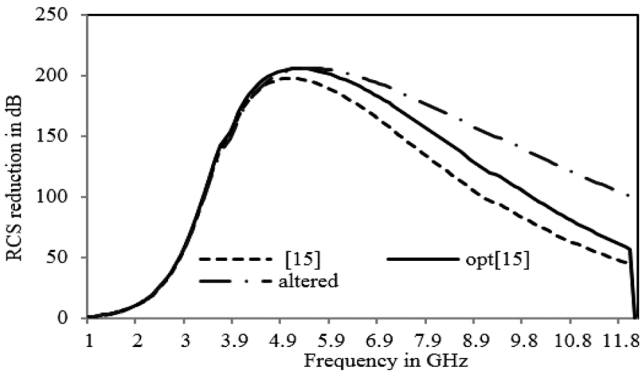

FIGURE 6 Reflection phase difference of the square-circle pair[15] optimized, and altered scenarios

TABLE 2 Dimensions of the Jerusalem cross

	Optimized (Rogers 3010)		Alternative (Taconic TLY-3 (1.57 mm) + air gap(3 mm))	
Jerusalem cross15	**Large (mm)**	**Small (mm)**	**Large (mm)**	**Small (mm)**
pl	1.76	0.93	11.4	1
pw	1.26	0.57	11.4	0.5
t,w	0.2	0.12	0.3	.2
p	4	4	15	15

initializing the unit cell dimensions. These initial values are used to activate CST and trigger the simulation. The simulated phase responses of the unit cells are extracted and returned to MATLAB. The bandwidth is estimated, and the dimensions of the unit cell for the next iteration are chosen based on the deviation from the fitness function. This cycle is iterated several times until fitness is achieved. This process is illustrated in Figure 2. In the process of optimization, one of the unit cell dimensions is initially fixed, and the other cell dimensions are varied. This approach has resulted in the bandwidth enhancement of previously reported structures.[14,15]

The next section describes the unit cells considered for the optimization problem and the dimensions obtained as a result of this process.

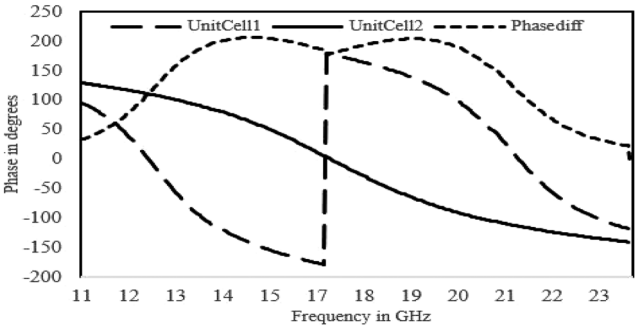

FIGURE 7 Phase response of the[14] optimized Jerusalem cross, large and small, and the phase difference between them

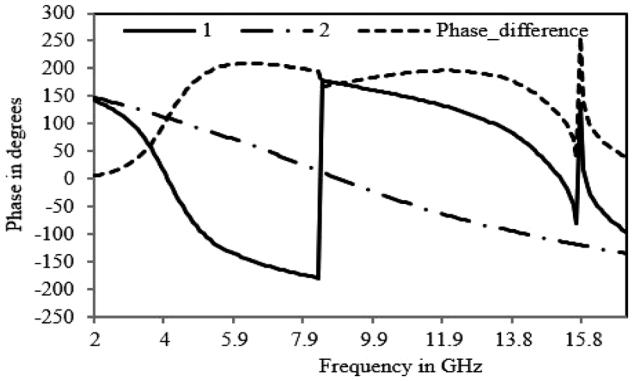

FIGURE 8 Phase response of the altered Jerusalem cross, unit cell 1 (large), unit cell 2 (small), and the phase difference between them

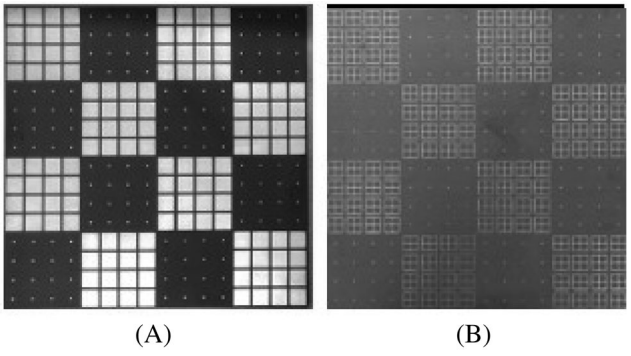

FIGURE 9 Fabricated metasurfaces A, square-circle-based checkerboard metasurface (CMS) and B, Jerusalem cross-based CMS

4 | DESCRIPTION OF THE UNIT CELLS

The unit cell pairs, square-circle (*a*) and Jerusalem cross (*b*), reported in References 14,15, respectively, are investigated for further bandwidth enhancement. Metasurface (a) reported in Reference 15 is designed on Rogers 5880 with a thickness of 6.35 mm, and metasurface (*b*) reported in Reference 14 is designed on Rogers 3010 with a thickness of 1.27 mm. The reported periodicity of the unit cell (*a*) is 15 mm, and that of (*b*) is 4 mm. Using the same configuration with the same periodicity, the elements (*a*) and (*b*) were optimized using the optimization procedure discussed in the previous section, resulting in enhanced bandwidth. The optimized dimensions are shown in Figure 3. The Jerusalem cross (JC) large-small, shown in Figure 4A,B is used to construct the CMS, where the two unit cells are the same in terms of element shape but have different geometrical dimensions, namely, large and small. The

FIGURE 10 Experimental setup

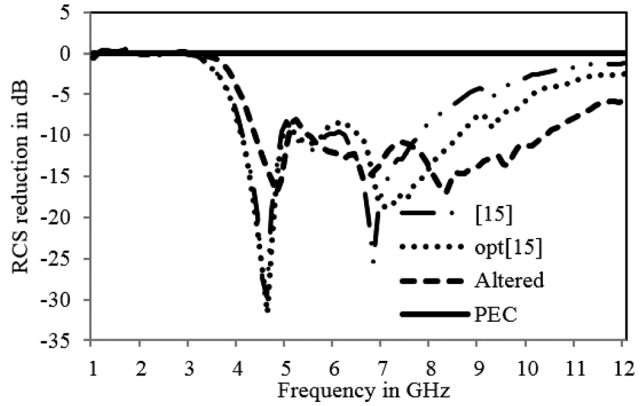

FIGURE 11 Simulated radar cross section (RCS) reduction for the square-circle pair[15] optimized, and altered checkerboard metasurface (CMS) scenarios

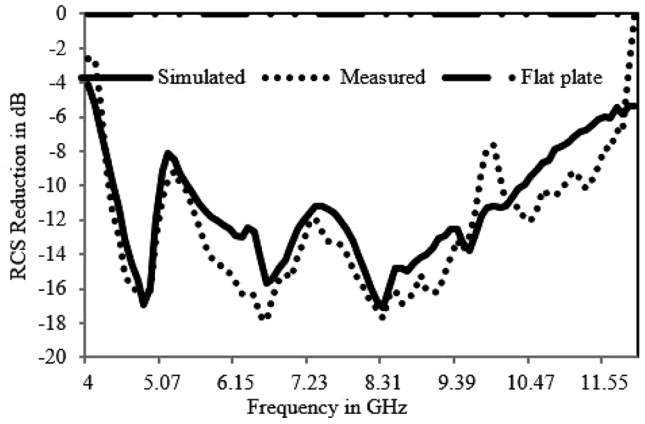

FIGURE 12 Monostatic radar cross section (RCS) reduction for the altered (vacuum + Taconic) square-circle checkerboard metasurface (CMS)

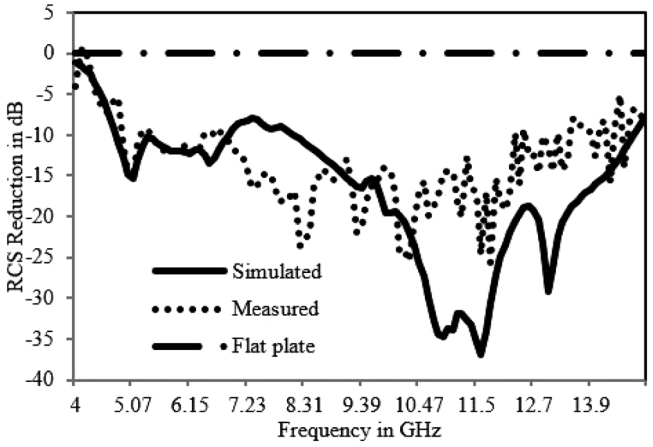

FIGURE 13 Monostatic radar cross section (RCS) reduction for the altered (vacuum+Taconic) Jerusalem cross checkerboard metasurface (CMS)

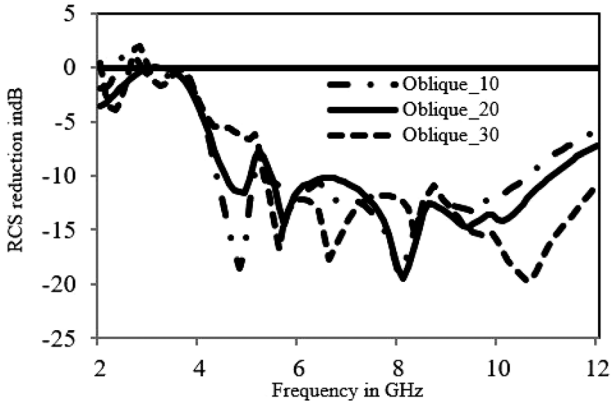

FIGURE 14 Simulated radar cross section (RCS) reduction for oblique incidences for the square-circle altered checkerboard metasurface (CMS)

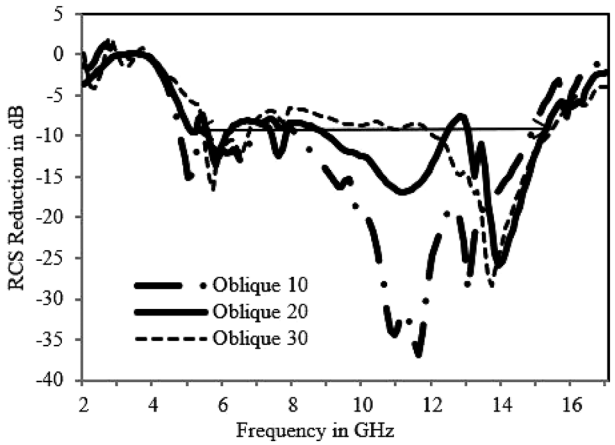

FIGURE 15 Radar cross section (RCS) reduction for different oblique incidences for the Jerusalem cross pair metasurface

TABLE 3 RCS reduction bandwidth for different incident angles

Oblique angles (degrees)	Altered square-circle fractional bandwidth (%)	Altered Jerusalem cross bandwidth (%)
10	82.7	101
20	65.8	74
30	77.4	25

Abbreviation: RCS, radar cross section.

optimized dimensions of JC that offer enhanced bandwidth are tabulated in Table 2.

To reduce the material cost and to explore an alternative method to enhance the bandwidth, the substrates in both (*a*) and (*b*) are replaced by Taconic TLY-3 of thickness 1.57 mm upon an air gap of 5 mm, as described in

Figure 5. For this altered configuration, the unit cell period considered is 15 mm for both (a) and (b). The optimized dimensions of (a) are the same as discussed earlier (a square with sides of 13.1 mm and a circle with 0.9 mm radius). The dimensions of (b) that provide enhanced bandwidth are mentioned in Table 2.

Since the alternate configuration considered in this work consists of a 5 mm air gap above which the Taconic TLY-3 is placed, determining the equivalent dielectric constant would be easier for comparison. The equivalent dielectric constant is determined using the expression reported in Reference 27 as follows.

$$\varepsilon_{\text{eff}} = \frac{d_1\varepsilon_{r1} + d_2\varepsilon_{r2}}{d_1 + d_2}, \tag{4}$$

where $d1$, $d2$ are the heights and ε_{r1}, $\varepsilon_{r2}$are the dielectric constants of the two layers. The estimated effective dielectric constant is 1.31 over a height of 6.57 mm. This has been included in the comparison table in the following section.

5 | RESULTS AND DISCUSSION

5.1 | Phase difference bandwidth

The square-circle pair in Reference 15 has been reported to offer a phase difference bandwidth of 63% (3.8-7.3 GHz). The same configuration on using the optimization procedure discussed in Section 3 offers an improved phase difference bandwidth of 70% (3.8-8.1 GHz). The unit cells designed using the altered substrate configuration further enhance the bandwidth to 80% over the frequency range of 3.8 to 9.2 GHz. Figure 6 shows the phase differences between the square and circle unit cells of the,[15] optimized,[15] and altered cases. The bandwidth corresponds to a phase deviation of $(180 \pm 37)^\circ$, as discussed in Section 2, which represents a -10 dB RCS reduction.

The Jerusalem cross pair reported in Reference 14 offered a phase difference bandwidth of 40%. After optimizing the same configuration, the phase difference bandwidth is 45%, as shown in Figure 7. Upon adopting alternative substrate-based unit cells and increased unit cell size, the frequency has shifted toward the lower band. This structure provides a substantial enhancement in bandwidth over the frequency range of 4.5 to 14.5 GHz (105%). The phase response of the unit cells and their phase differences are shown in Figure 8.

5.2 | Simulated and measured RCS reduction of CMS

Based on the unit cell dimension obtained from the optimization algorithm, two AMC arrays are constructed using 4×4 unit cells, which in turn are placed in a checkerboard fashion to construct a 240 mm × 240 mm metasurface. The alternate configuration using the Taconic substrate with an air gap is fabricated, which is shown in Figures 9A,B. The measurements are performed at the authors' institution. Owing to the limitations of the measurement setup, only the monostatic RCS is measured, whereas the simulation results of both the monostatic and bistatic cases are discussed. The measurement setup is elaborated as follows.

5.2.1 | Measurement setup

RCS reduction measurement setup demonstrated for periodic structures in Reference 28, reports the reflection

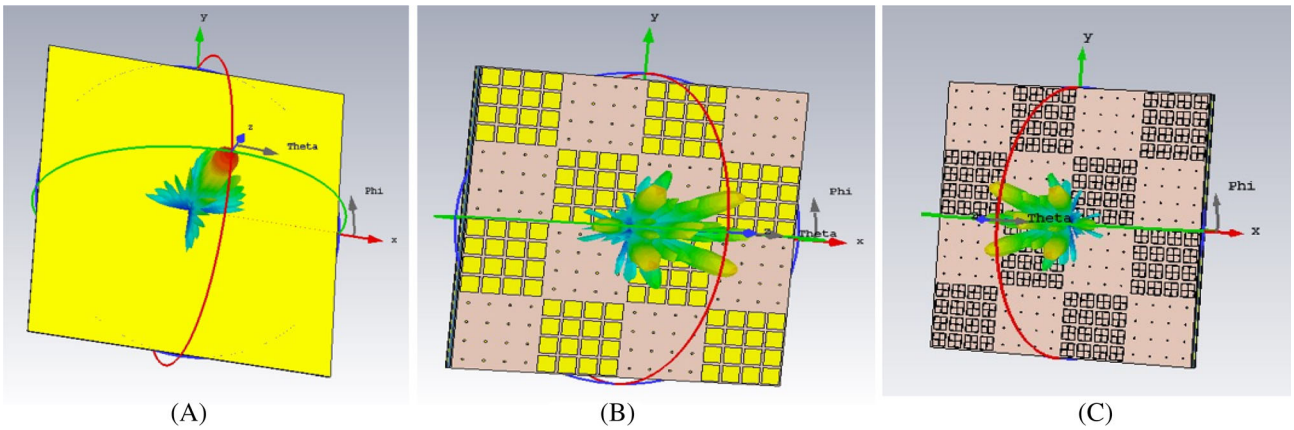

(A) (B) (C)

FIGURE 16 3D simulated scattering pattern at 7.5 MHz A, flat metal plate, B, square circle based checkerboard metasurface (CMS), and C, Jerusalem cross based CMS

amplitude reduction as being similar to that of RCS reduction. A similar measurement setup is considered in this work. The RCS measurement is carried out in an outdoor setup at the author's institution, as indicated in Figure 10.

Two identical horn antennas, operating from 2 to 18 GHz, are used as the transmitting and receiving antennas. These antennas are connected to the ports of the network analyzer, and S_{21} is measured. A power amplifier is used to boost the transmit power from 4 to 20 dBm over the frequency range 2 to 18 GHz. Although a power amplifier is used, the amplification is not sufficient to reach large distances corresponding to the far-field. Hence, the separation between the CMS panel and the Tx/Rx horn is maintained at 2 m rather than a representative far-field distance (7 m) at the highest frequency of the metasurface aperture.

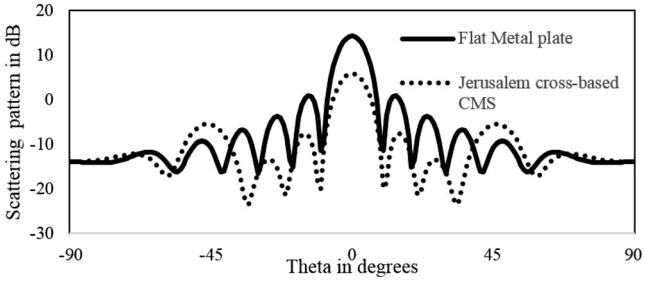

FIGURE 17 2D scattering pattern of flat metal plate and JC-based checkerboard metasurface (CMS) at 7.5 GHz

5.2.2 | Monostatic RCS

Square-circle pair: Figure 11 shows the simulated monostatic RCS of Reference 15 after optimization and the altered metasurface scenarios. The bandwidth is improved to 70% (4.1-8.6 GHz) using the optimized dimensions. Additionally, the bandwidth for the altered case further enhances to 81% over the frequency range 4.4 to 10.4 GHz.

The Taconic-based square-circle CMS shows a good match between the simulation and measurement results, as depicted in Figure 12. The fractional bandwidth obtained through simulations is 81%. On observing the measured results, the stringent − 10 dB bandwidth obtained is 75% over the frequency range 4.35 to 9.66 GHz. However, including a spike of 8 dB within 10 dB, the bandwidth expands to 88% over the frequency range 4.35 to 11.28 GHz.

Jerusalem cross pair: The simulation of the Jerusalem cross-based CMS on a Taconic substrate results in a considerable increase in the RCS reduction bandwidth to approximately 102%, as shown in Figure 13. The simulated 15 dB bandwidth is 48%, which is the widest that has been reported so far. The measured 10 dB bandwidth is 98% (4.89-14.3 GHz), and the 15 dB bandwidth (with 14 dB spikes) is 50% (7.3-12.2 GHz).

Even though a phase deviation of $(180 \pm 37)^{\circ}$ is maintained between the unit cells, the overall CMS simulation shows an 8.5 dB spike at 5.5 GHz for the square-circle pair and an 8 dB spike at approximately 7 to 8 GHz for the Jerusalem cross pair. The same behavior was

TABLE 4 Performance comparison with similar works

Ref. no./Year of Publication	Thickness of substrate (mm)	ε_r/ ε_{eff}	Period (mm)	− 10 dB RCS Reduction Bandwidth in GHz (fractional bandwidth)		− 15 dB RCS Reduction frequency range in GHz (fractional bandwidth) Simulated
				Simulated	Measured	
12/2011	2	2.65	8	4.9-7.9(46.8%)[a]	5.1-7.5(32%)	5.2-5.45(4.6%)
13/2013	1.27	10.2	4	14.4-21.8(41%)	14.8 to 22.7 (42%)	15.1-17.0(12.5%)
14/2015	6.35	2.2	15	4.2-7.9(61%)	4.2-7.8(60%)	4.25-4.8(12%)
15 / 2016	6.35	2.2	14	3.94-7.4(61%) 8.41-10.72(24%)	3.94-7.4(61%) 8.41-10.72(24%)	6.4-6.7(4%) 8.9-9.5(3%)
16/2017	6.35	2.2	14	3.75-10(91%)	3.75-10(91%)	4.1-4.9(17%) 8.3-9.3(11%)
17/2019	11(vacuum) +.5 (substrate)	3.48/1.1	11	3.78-10.08 (90.9%)	3.77-10.14(91.5%)	3.9-4.5(14%) 5.8-7.5(25%)
18/2019	3.175	2.2	15	8-16(66.7%)	7.98-16.32(68.6%)	11.6-16(31%)
This work (Jerusalem cross)	5 (vacuum) +1.57 (substrate)	2.33/1.3	15	4.8–14.8(102%)	4.89–14.3(98%)	(9.1-14.2)48%

Abbreviation: RCS, radar cross section.

[a]– 6 dB bandwidth.

previously reported in References 13,14, where the cause has been discussed as the diffraction effects of the finite edges. This behavior can also be attributed to mutual coupling between adjacent cells.

5.2.3 | Bistatic RCS

The simulated bistatic RCS reduction for oblique incidences of 10°, 20°, and 30° are shown in Figures 14 and 15 for the altered configurations of (*a*) and (*b*), respectively. It is observed that the bandwidth offered decreases with an increase in the angle of incidence. Table 3 provides the bandwidth offered by the metasurfaces in the bistatic case.

5.2.4 | Scattering patterns

The 3D scattering patterns of both the reported structures (a) square-circle pair, and (b) Jerusalem cross pair are shown in Figure 16. The scattering from a flat metal plate is shown in Figure 16A, which conveys the scattering to be very high in the transmitter's direction. Once the CMS is introduced, the scattering is reduced, as shown in Figure 16B,C. The 2D scattering pattern of flat metal plate and that of Jerusalem cross based CMS is shown in Figure 17.

6 | COMPARISON WITH SIMILAR WORKS

The Jerusalem cross pair designed on Taconic TLY-3 with an air gap offers a substantial increment in the bandwidth. Hence, the CMS built using the altered Jerusalem cross is compared with previously reported similar works. Additionally, the 15 dB RCS reduction bandwidth obtained is 48%. This is the widest 15 dB RCS reduction bandwidth reported so far. The comparison is made with similar works reported on a single substrate with or without an air gap. A comparison of the current work with related previously published works is tabulated in Table 4.

7 | CONCLUSION

In this work, an IFOA-based optimization approach was proposed for further enhancing the bandwidth of wideband RCS reduction for CMSs. Two previously published structures were chosen: (a) a square-circle unit cell pair on Rogers 5880 with a thickness of 6.35 mm and (b) a Jerusalem cross unit cell pair on Rogers 3010 with a thickness of 1.27 mm. After optimization, these unit cells showed a 7% increase in bandwidth in the case of (*a*) and 5% in the case of (*b*). Owing to the cost of the substrate and in light of exploring an alternate method, the substrates in both (*a*) and (*b*) were replaced by Taconic TLY-3 with a thickness of 1.57 mm over an air gap of 5 mm. The simulation results showed a significant improvement in the − 10 dB RCS reduction bandwidth: 81% (4.4-10.4 GHz) in the case of (*a*), and 102% (4.8-14.8 GHz) in the case of (*b*). The − 15 dB bandwidth of structure (*b*) was 48% (9.1-14.2 GHz) which is widest reported so far. The RCS measurements closely matched the simulation results.

DATA AVAILABILITY STATEMENT

The authors have the data corresponding to the plots included in the manuscript. On request to the first author, these data can be shared.

ORCID

Akila Murugesan https://orcid.org/0000-0002-7565-2316
Krishnasamy T. Selvan https://orcid.org/0000-0002-0467-4841

REFERENCES

1. Knott E, Shaeffer J, Tuley M. *Radar Cross Section*. Raleigh, NC, USA: SciTech Pub.; 2004.
2. Kern DJ, Werner DH. A genetic algorithm approach to the design of ultra-thin electromagnetic bandgap absorbers. *Microw Opt Technol Lett*. 2003;38:61-64.
3. Zhang Y, Mittra R, Wang BZ, Huang NT. AMC's for ultra-thin and broadband RAM design. *Electron Lett*. 2009;45:484-485.
4. Salisbury WW. Absorbent Body for Electromagnetic Waves. US Patent No. 2599944 A; 1952.
5. Bondeson A, Yang Y, Weinerfelt P. Shape optimization for radar cross sections by a gradient method. *Int J Numer Meth Eng*. 2004;61:687-715.
6. Yu N, Genevet P, Kats MA, et al. Light propagation with phase discontinuities: generalized laws of reflection and refraction. *Science*. 2011;333-337.
7. Li Y, Zhang J, Qu S, et al. Wideband radar cross section reduction using two-dimensional phase gradient metasurfaces. *Appl Phys Lett*. 2014;104:221110.
8. Zhuang Y, Wang G, Liang J, et al. Random combinatorial gradient metasurface for broadband, wide-angle and polarization-independent diffusion scattering. *Nature, Sci Rep*. 2017;7:16560.
9. Dai H, Zhao Y, Chen J, Yu C, Xing L. Ultra wideband radar cross section reduction using polarization conversion metasurface. *Int J RF Microw Comput Aid Eng*. 2019.
10. Akbari M, Samadi F, Sebak A, Denidni TA. Superbroadband diffuse wave scattering based on coding metasurfaces: polarization conversion metasurfaces. *IEEE Antennas Propag Mag*. 2019;61:40-52.
11. Paquay M, Iriarte J, Ederra I, Gonzalo R, de Maagt P. Thin AMC structure for radar cross-section reduction. *IEEE Trans Antennas Propag*. 2007;55:3630-3638.

12. de Cos ME, Alvarez Y, Las-Heras F. A novel approach for RCS reduction using a combination of artificial magnetic conductors. *Prog Electromagn Res*. 2010;107:147-159.
13. Fu Y, Li Y, Yuan N. Wideband composite AMC surfaces for RCS reduction. *Microw Opt Technol Lett*. 2011;53:712-715.
14. Galarregui JCI, Pereda AT, de Falcón JLM, Ederra I, Gonzalo R, Maagt P. Broadband radar cross-section reduction using AMC technology. *IEEE Trans Antennas Propag*. 2013;61:6136-6143.
15. Chen W, Balanis CA, Birtcher CR. Checkerboard EBG surfaces for wideband radar cross section reduction. *IEEE Trans Antennas Propag*. 2015;63:2636-2645.
16. Chen W, Balanis CA, Birtcher CR. Dual wide-band checkerboard surfaces for radar cross section reduction. *IEEE Trans Antennas Propag*. 2016;64:4133-4138.
17. Modi AY, Balanis CA, Birtcher CR, Shaman HN. Novel design of ultrabroadband radar cross section reduction surfaces using artificial magnetic conductors. *IEEE Trans Antennas Propag*. 2017;65:5406-5417.
18. Sang D, Chen Q, Ding L, Guo M, Fu Y. Design of Checkerboard AMC structure for wideband RCS reduction. *IEEE Trans Antennas Propag*. 2019;67:2604-2612.
19. Kim SH, Yoon YJ. Wideband radar cross-section reduction on checkerboard metasurfaces with surface wave suppression. *IEEE Antennas Wirel Propag Lett*. 2019;18:896-900.
20. Zaker R, Sadeghzadeh A. Wideband radar cross section reduction using a novel design of artificial magnetic conductor structure with a triple layer chessboard configuration. *Int J RF Microwave Comput Aid Eng*. 2018;e21545. https://doi.org/10.1002/mmce.21545.
21. Murugesan A, Natarajan D, Selvan KT. Low-cost, wideband checkerboard metasurfaces for monostatic RCS reduction. *IEEE Antennas and Wirel Propag Lett*. 2021;20(4):493–497. https://doi.org/10.1109/LAWP.2021.3054863.
22. Lu Y, Su J, Liu J, et al. Ultrawideband Monostatic and Bistatic RCS reductions for both Copolarization and cross polarization based on polarization conversion and destructive interference. *IEEE Trans Antennas Propag*. 2019;67:4936-4941.
23. Akila M, Anusha P, Sindhu M, Selvan KT. Examinations on PSO, GA-PSO, ACO algorithms for the design optimization of printed antennas. *Proc IEEE Appl Electromagn Conf (AEMC)*. 2017.
24. Darvish A, Ebrahimzadeh A. Improved fruit-Fly optimization algorithm and its applications in antenna arrays synthesis. *IEEE Trans Antennas Propag*. 2018;66:1756-1766.
25. Modi AY, Balanis CA, Birtcher CR, Shaman HN. New class of RCS-reduction Metasurfaces based on scattering cancellation using Array theory. *IEEE Trans Antennas Propag*. 2019;67:298-308.
26. https://tensorbundle.wixsite.com/home Accessed on 25-March-2020
27. Costa F, Monorchio A, Manara G. Efficient analysis of frequency-selective surfaces by a simple equivalent-circuit model. *IEEE Antennas Propag Mag*. 2012;54(4):35-48. https://doi.org/10.1109/MAP.2012.6309153.
28. Álvarez Y, Elena de Cos M, Las-Heras F. RCS measurement setup for periodic-structure prototype characterization. *IEEE Antennas Propag Mag*. 2010;52(3):100-106. https://doi.org/10.1109/MAP.2010.5586586.

AUTHOR BIOGRAPHIES

Ms. Akila Murugesan, completed her B.E degree in Electronics and Communication from Anna University at MEPCO Schlenk Engineering College, India in 2005 and was awarded a gold medal for standing first in college. She received her M.E degree in Communication Systems from Anna University at SSN College of Engineering, India in 2008 and ranked fourth at this institute. Her professional career spanned eight years during which she worked in the software industry for four years and in academics for another four years. She is currently doing her Ph. D in the Department of Electronics and Communication Engineering at SSN College of Engineering, India. She is pursuing her research on metasurfaces for RCS reduction.

Her professional interests include electromagnetics, antenna and computational electromagnetics. She is a student member of IEEE.

Dr. Krishnasamy T. Selvan received the B.E. (Honours) degree from the Madurai Kamaraj University in 1987, the MS degree from the Birla Institute of Technology and Science Pilani in 1996 and the PhD degree from the Jadavpur University, Kolkata in 2002. He has been a Professor in the Department of Electronics & Communication Engineering, SSN College of Engineering, India since June 2012. From February 2005 to early June 2012, he was with the Department of Electrical & Electronic Engineering, University of Nottingham Malaysia Campus. From January 1988 to early February 2005, he was with SAMEER – Centre for Electromagnetics, Chennai. He was a UNDP Fellow at RFI Industries, Australia, early 1994 and a Visiting Scholar at the George Green Institute for Electromagnetic Research, University of Nottingham, UK in late 2008.

Selvan's professional interests include electromagnetics, electromagnetics education, antenna theory, design and measurements, printed antennas and arrays, and rcs reduction techniques. In these areas, he has authored or co-authored a number of journal and conference papers. He is also interested in keenly reflecting about professional development and ethics. Selvan was on the Editorial Board of the International Journal of RF and Microwave Computer Aided Engineering from 2006 to 2011. He founded the Madras

Chapter of IEEE Antennas and Propagation Society (AP-S) in 2013. He has been involved in several major conferences and workshops, both as a speaker and as an organizer. He was a member of the Education Committee of the IEEE AP-S from 2006 to 2018. On an invitation from IEEE AP-S Taiwan Chapter, he visited National Taiwan University in July 2016 and gave a talk on his experience in promoting EM education in South India.

The book "Teaching electromagnetics: Innovative approaches and pedagogical strategies" that Selvan has co-edited with Professor Karl Warnick, BYU, USA is to be published mid-2021 by the CRC Press.

How to cite this article:
Murugesan ASelvan KTOn further enhancing the bandwidth of wideband RCS reduction checkerboard metasurfaces using an optimization algorithm. *Int J RF Microw Comput Aided Eng*. 2021;31:e22686. https://doi.org/10.1002/mmce.22686